Journal of Power Sources 240 (2013) 95–100

Contents lists available at SciVerse ScienceDirect

Journal of Power Sources

journal homepage: www.elsevier.com/locate/jpowsour

Short communication

Synthesis and electrochemical properties of $LiNi_{0.5-x}Cu_xMn_{1.5-y}Al_yO_4$ ($x = 0, 0.05, y = 0, 0.05$) as 5 V spinel materials

Jianhong Liu [a,b,*], Zhaoqin Sun [b], Jiaona Xie [b], Hongyu Chen [b], Ningning Wu [b], Borong Wu [a]

[a] School of Chemical Engineering and Environment, Beijing Institute of Technology, Beijing 100081, China
[b] CITIC Guoan Mengguli Power Science and Technology Co., Ltd, Beijing 102200, China

HIGHLIGHTS

- The doped $LiNi_{0.5}Mn_{1.5}O_4$ spinels were synthesized using different cation as dopant.
- The doping effect and mechanism of Al^{3+} and Cu^{2+} is found to be different.
- Both Al^{3+} and Cu^{2+} doping can improve electrochemical property of $LiNi_{0.5}Mn_{1.5}O_4$.
- Co-doped $LiNi_{0.45}Cu_{0.05}Mn_{1.45}Al_{0.05}O_4$ exhibited the best cyclic performance.

ARTICLE INFO

Article history:
Received 3 February 2013
Received in revised form
25 March 2013
Accepted 29 March 2013
Available online 9 April 2013

Keywords:
Co-doped
Electrochemical performance
Doping effect
Capacity retention

ABSTRACT

The $LiNi_{0.5-x}Cu_xMn_{1.5-y}Al_yO_4$ ($x = 0, 0.05, y = 0, 0.05$) powders are synthesized by liquid co-precipitation and wet-milling. The doping effect on $LiNi_{0.5}Mn_{1.5}O_4$ by Al^{3+}, Cu^{2+}, and Al^{3+}/Cu^{2+} co-doping are investigated and compared in relation to physical and electrochemical characterization, namely, through X-ray diffraction, scanning electron microscopy, electronic conductivity, cyclic voltammetry and cycle tests. Results suggest that both Al^{3+} and Cu^{2+} doping effectively improve electrochemical performance of $LiNi_{0.5}Mn_{1.5}O_4$, although the effect is different between the two cations. All doped samples exceed 95% capacity retention after 100 cycles at room temperature compared to 92% retention for the undoped sample. Moreover, co-doped $LiNi_{0.45}Cu_{0.05}Mn_{1.45}Al_{0.05}O_4$ exhibits the best cyclic performance with slight superiority.

© 2013 Elsevier B.V. All rights reserved.

1. Introduction

Spinel lithium manganese oxide ($LiMn_2O_4$) has received increasing attention as a cathode in lithium-ion batteries for electric and hybrid electric vehicles due to its low cost, low toxicity, and relatively high energy density [1–3]. Spinel $LiMn_2O_4$ with *Fd*-3m space group provides a 3D network for Li^+ ion diffusion, which increases the speed of Li^+ ion insertion and deinsertion during charging–discharging [4–10]. However, poor cyclic behavior at elevated temperatures restrains the application of $LiMn_2O_4$ in Li-ion batteries [11–14]. To solve this problem, modification research has been conducted on Mn-substitution by other cations to prepare $LiM_xMn_{2-x}O_4$ (M = Al, Co, Cr, Ni, Fe, Cu) [15–20].

Among these spinel materials, $LiNi_{0.5}Mn_{1.5}O_4$ has been considered the most important and attractive due to its relatively good cycling behavior and relatively high capacity [21,22]. When $LiNi_{0.5}Mn_{1.5}O_4$ is charged to 5 V, there is a higher voltage plateau between 4.5 and 4.9 V corresponding with Ni^{2+}/Ni^{4+} redox reaction in an [MO_6] octahedron framework after deintercalation of Li^+, which gives it a higher energy density than $LiMn_2O_4$ [23]. Moreover, $LiNi_{0.5}Mn_{1.5}O_4$ has two different crystal structures of the *Fd*-3m space groups (non-stoichiometric disordered $LiNi_{0.5}Mn_{1.5}O_4$), in which Mn ions are present as mainly Mn^{4+} with little Mn^{3+}, and $P4_332$ stoichiometric ordered $LiNi_{0.5}Mn_{1.5}O_4$, in which Mn ions are only present in Mn^{4+} [24]. The disordered $LiNi_{0.5}Mn_{1.5}O_4$ spinel was found to have better electrochemical performance than the ordered spinel $LiNi_{0.5}Mn_{1.5}O_4$ [25]. Non-stoichiometric $LiNi_{0.5}Mn_{1.5}O_4$ has the same crystal structure as pure spinel $LiMn_2O_4$, that is, a face-centered cubic structure with the *Fd*-3m space group, the Ni and Mn, Li and O atoms occupied in the 16d octahedral sites, 8a tetrahedral sites, and 32e sites, respectively. In this case, Ni and Mn atoms are randomly distributed in the 16d sites [26]. When all lithium-ions are extracted from $LiNi_{0.5}Mn_{1.5}O_4$, the theoretical capacity is 147 mAh g^{-1}. However, capacity fading during cycling may also exist due to structural and chemical instabilities resulting from the presence of high spin Mn^{3+} ions [27].

* Corresponding author. School of Chemical Engineering and Environment, Beijing Institute of Technology, Beijing 100081, China. Tel./fax: +86 010 89702984.
E-mail address: ljhmgl@yahoo.com.cn (J. Liu).

0378-7753/$ – see front matter © 2013 Elsevier B.V. All rights reserved.
http://dx.doi.org/10.1016/j.jpowsour.2013.03.172

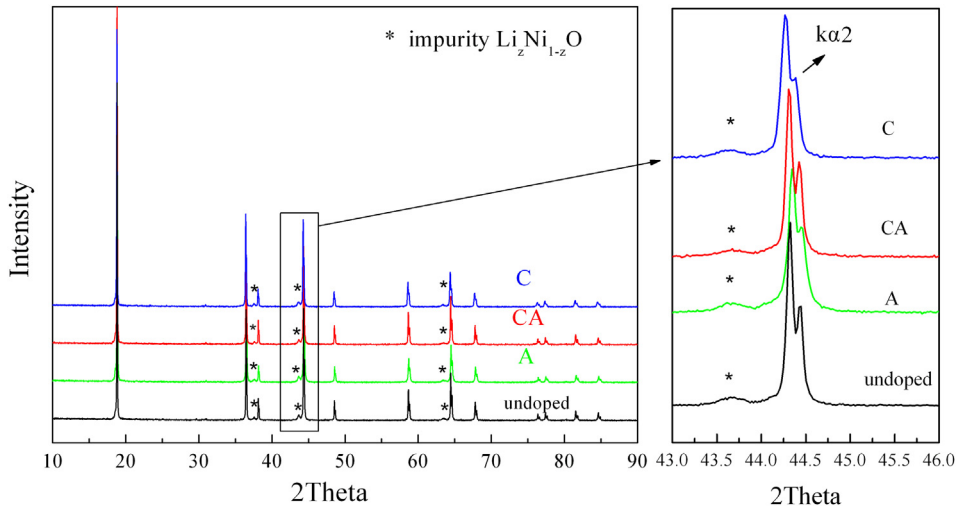

Fig. 1. X-ray diffraction patterns of $LiNi_{0.5-x}Cu_xMn_{1.5-y}Al_yO_4$ ($x = 0, 0.05$, $y = 0, 0.05$): C is $LiNi_{0.45}Cu_{0.05}Mn_{1.5}O_4$, CA is $LiNi_{0.45}Cu_{0.05}Mn_{1.45}Al_{0.05}O_4$, and A is $LiNi_{0.5}Mn_{1.45}Al_{0.05}O_4$.

Many modification studies have been conducted to improve the electrochemical performance of $LiNi_{0.5}Mn_{1.5}O_4$, including doping and surface coating. Among these $LiNi_{0.5}Mn_{1.5}O_4$ modification methods, Al^{3+} doping and Cu^{2+} doping have received considerable attention. Al-doping can effectively increase structure stability to improve cyclic performance due to stronger bond energy for Al—O compared with Mn—O and Ni—O [12,28]. Cu-doping can increase electronic conductivity due to the special outer electronic arrangement of Cu^{2+} [29,30]. Double cation or multi-doping methods have a possible synergistic effect to improve the cycling life of the materials as cathodes in lithium batteries [4,31–35].

In this study, $LiNi_{0.5-x}Cu_xMn_{1.5-y}Al_yO_4$ ($x = 0, 0.05$, $y = 0, 0.05$) materials were synthesized by liquid co-precipitation and wet-milling for well mixing-dispersive effects compared to solid state processes [3]. Physical and electrochemical performance of these spinels were characterized and investigated by XRD, particle distribution, SEM, cyclic voltammetry, and cyclic life test. Performance differences among Al^{3+}/Cu^{2} co-doping spinels, single Al^{3+} or Cu^{2+} doping spinels, and undoped $LiNi_{0.5}Mn_{1.5}O_4$ were investigated. The Al^{3+}/Cu^{2+} co-doping $LiNi_{0.45}Cu_{0.05}Mn_{1.45}Al_{0.05}O_4$ was found to have the best cyclic performance.

2. Experimental

2.1. Synthesis of $LiNi_{0.5-x}Cu_xMn_{1.5-y}Al_yO_4$ powders

The $LiNi_{0.5-x}Cu_xMn_{1.5-y}Al_yO_4$ ($x = 0, 0.05$, $y = 0, 0.05$) powders were synthesized by liquid co-precipitation and wet-milling processes. Stoichiometric amounts of $MnSO_4 \cdot H_2O$, $NiSO_4 \cdot 6H_2O$, $CuSO_4 \cdot 5H_2O$, and $Al(NO)_3$ were dissolved in deionized water to obtain a homogeneous solution and then were precipitated by NaOH solution. The pH value was adjusted to around 10.5 during the precipitation reaction by addition of ammonium hydroxide (NH_4OH) solution. The collected precipitate was isolated by vacuum filtration, washed several times with deionized water, and then dried inside an oven at 100 °C for several hours. The precipitates were mixed with lithium source Li_2CO_3 at the designed stoichiometry using ethanol as dispersant, and then calcined at 950 °C for 12 h in air to obtain $LiNi_{0.5-x}Cu_xMn_{1.5-y}Al_yO_4$ powders.

2.2. Characterization and electrochemical test of powders

X-ray diffraction (XRD) patterns of $LiNi_{0.5-x}Cu_xMn_{1.5-y}Al_yO_4$ ($x = 0, 0.05$, $y = 0, 0.05$) powders were collected on a Bruker D8 ADVANCE Powder Diffractometer with Cu Kα radiation ($\lambda = 1.5406$ Å) between 10 and 90° (40 kV, 40 mA, step size = 0.02° and a count time of 0.2 s/step.) in order to identify the crystalline phase of the materials. Rietveld refinements of the crystal parameter for all samples were performed using Bruker Topas4.2 software. Particle morphologies of $LiNi_{0.5-x}Cu_xMn_{1.5-y}Al_yO_4$ ($x = 0, 0.05$, $y = 0, 0.05$) were examined by field-emission scanning electron microscopy (FSEM) on a Hitachi S-4800 instrument (Japan). Electronic conductivities of all powders were carried out on a conductivity meter (Shanghai SB118, China) using a conventional four-point probe method. Particle size distributions of the powders were identified by a laser particle size analyzer (Beckman LS32, America).

Electrodes were made by casting a slurry of 90% weight active material oxide, 5% conductive reagent (Timcal, super-P), and 5% PVDF binder (Kynar) in *N*-methyl-2-pyrollidinone (NMP) solvent onto an Al foil substrate. The slurry was cast by a doctor blade. The cast laminates were firstly dried in air at 120 °C for 2 h, and then in vacuum at 70 °C for 8 h. They were then pressed to a fixed thickness of 80–100 μm, and each electrode had the same weight of active matter (6.6 ± 0.2 mg). Lithium coin cells (CR2032) were fabricated in an Ar filled glove box (<1 ppm O_2), with lithium metal as the anode, Celgard 2400 microporous polypropylene membrane as the separator and an electrolyte comprised of 1 M $LiPF_6$ in a 1:1:1 volume fraction of ethylene carbonate (EC)/dimethyl carbonate (DMC)/ethyl–methyl carbonate (EMC). Cyclic voltammetry (CV) spectrums were investigated at a 50 μV s^{-1} scan rate, with a scan range of 3.0–5.0 V on a ZAHNER-IM6eX electrochemical workstation (Germany) at room temperature. Area specific impedance (ASI) measurements were carried out using a 10 s current interruption method every 30 min during the charge/discharge course. Charge–discharge performances were investigated using a CT2001A battery

Table 1
The electronic conductivity and crystal structural parameters of $LiNi_{0.5-x}Cu_xMn_{1.5-y}Al_yO_4$ powders.

Sample name	Theoretical chemical formula	a (Å)	V (Å^3)	Rwp	Electronic conductivity (S cm^{-1})
A	$LiNi_{0.5}Mn_{1.45}Al_{0.05}O_4$	8.1707	545.49	11.41	4.1E-06
C	$LiNi_{0.45}Cu_{0.05}Mn_{1.5}O_4$	8.1817	547.68	10.89	1.8E-05
CA	$LiNi_{0.45}Cu_{0.05}Mn_{1.45}Al_{0.05}O_4$	8.1759	546.52	11.58	1.1E-05
Undoped	$LiNi_{0.5}Mn_{1.5}O_4$	8.1746	546.26	11.36	6.3E-06

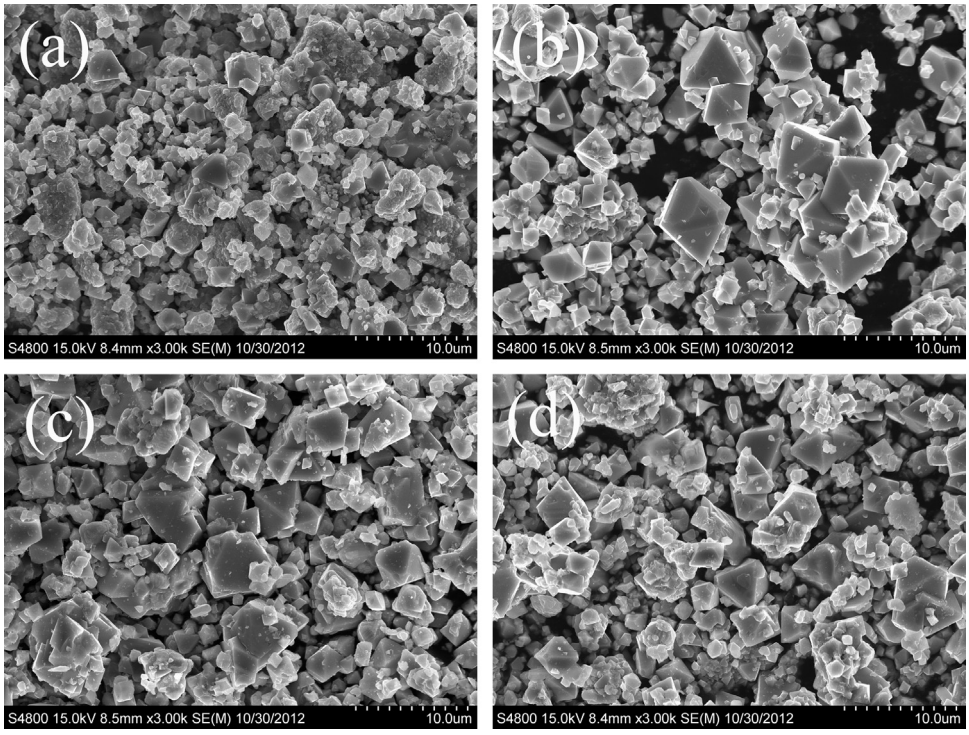

Fig. 2. SEM images of $LiNi_{0.5-x}Cu_xMn_{1.5-y}Al_yO_4$ ($x = 0, 0.05$, $y = 0, 0.05$): (a) $LiNi_{0.5}Mn_{1.45}Al_{0.05}O_4$, (b) $LiNi_{0.45}Cu_{0.05}Mn_{1.5}O_4$, (c) $LiNi_{0.45}Cu_{0.05}Mn_{1.45}Al_{0.05}O_4$ and (d) undoped $LiNi_{0.5}Mn_{1.5}O_4$.

tester (Land@, China) within voltage windows selected between a maximum 5.0 V and a minimum 3.0 V at 25 °C.

3. Results and discussion

3.1. XRD spectroscopy and particle morphology

Fig. 1 shows the XRD patterns of $LiNi_{0.5-x}Cu_xMn_{1.5-y}Al_yO_4$ ($x = 0$, 0.05, $y = 0$, 0.05) spinels. All samples were identified as having a cubic structure with *Fd*-3m space group. Some impurity peaks were detected at 43.6°, 37.5° and 63.5°, which were identified as $Li_{z-}Ni_{1-z}O$ in earlier literature [36,37], but attributed to another impurity of manganese-rich oxide with rock-salt structure in later research [38]. The right graph of Fig. 1 shows that compared with undoped $LiNi_{0.5}Mn_{1.5}O_4$, the diffraction peak shifted to a low angle direction for $LiNi_{0.45}Cu_{0.05}Mn_{1.5}O_4$ with Cu^{2+} doping, in contrast to a large angle direction for $LiNi_{0.5}Mn_{1.45}Al_{0.05}O_4$ with Al^{3+} doping, which accords with previous findings [39,40]. For Cu^{2+}/Al^{3+} co-doped spinel $LiNi_{0.45}Cu_{0.05}Mn_{1.45}Al_{0.05}O_4$, the crystal lattice parameter was 8.1759 Å (Table 1). It was expected that the crystal lattice parameter of Cu^{2+}/Al^{3+} co-doped spinel was between the parameter 8.1817 Å of Cu^{2+} single doped sample and 8.1707 Å of Al^{3+} single doped sample. This was considered to be related to the ionic radius relationship of Cu^{2+} (0.73 Å), Al^{3+} (0.535 Å), Ni^{2+} (0.69 Å), and Mn^{4+} (0.60 Å) [29,30,41].

Table 1 shows the rank of electronic conductivity of $LiNi_{0.5-x}Cu_xMn_{1.5-y}Al_yO_4$ powders as C > CA > undoped > A. This suggests that Cu^{2+} doping effectively increased the electronic conductivity of 5 V spinel $LiNi_{0.5}Mn_{1.5}O_4$ because Cu^{2+} ions participate in the electron transport process [29,30]. Whereas, the electronic conductivity of $LiNi_{0.5}Mn_{1.45}Al_{0.05}O_4$ with Al^{3+} doping was lower than undoped $LiNi_{0.5}Mn_{1.5}O_4$ because no electronic cloud overlap exists in the outer electronic shell between Al^{3+} and Mn^{4+}. The similar regularity about electronic conductivity is present compared with $LiMn_{2-x}Al_xO_4$ spinels [41].

Fig. 2 shows the scanning electron microscopy images of $LiNi_{0.5-x}Cu_xMn_{1.5-y}Al_yO_4$ ($x = 0$, 0.05, $y = 0$, 0.05). When doped with Al^{3+}, particle sizes became smaller compared to undoped $LiNi_{0.5}Mn_{1.5}O_4$. In the case of Cu^{2+} doped $LiNi_{0.45}Cu_{0.05}Mn_{1.5}O_4$, the particle size was relatively larger. A moderate particle size was obtained for $LiNi_{0.45}Cu_{0.05}Mn_{1.45}Al_{0.05}O_4$ co-doped with Cu^{2+}/Al^{3+} ions. In terms of the same sintering method for all samples, it was presumed that the Cu^{2+} ion had an enhancing effect on sintering, whereas the Al^{3+} ion had a restraining effect on the particle growth of $LiNi_{0.5}Mn_{1.5}O_4$, which reduced Li^+ ion migration resistance and increased high drain capability.

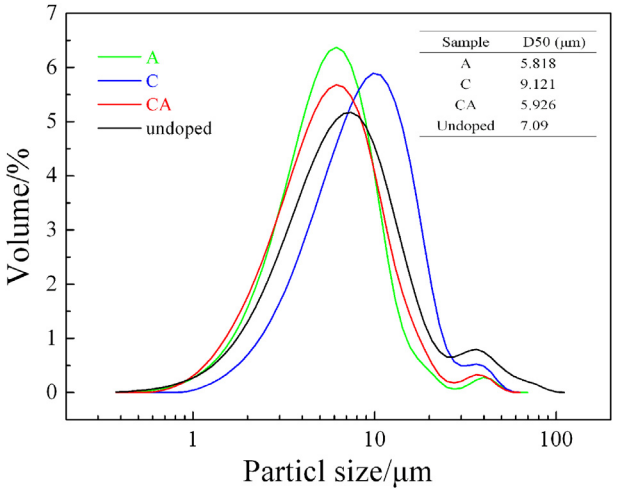

Fig. 3. Particle size distributions of $LiNi_{0.5-x}Cu_xMn_{1.5-y}Al_yO_4$ ($x = 0$, 0.05, $y = 0$, 0.05): A is $LiNi_{0.5}Mn_{1.45}Al_{0.05}O_4$, C is $LiNi_{0.45}Cu_{0.05}Mn_{1.5}O_4$, and CA is $LiNi_{0.45}Cu_{0.05}Mn_{1.45}Al_{0.05}O_4$.

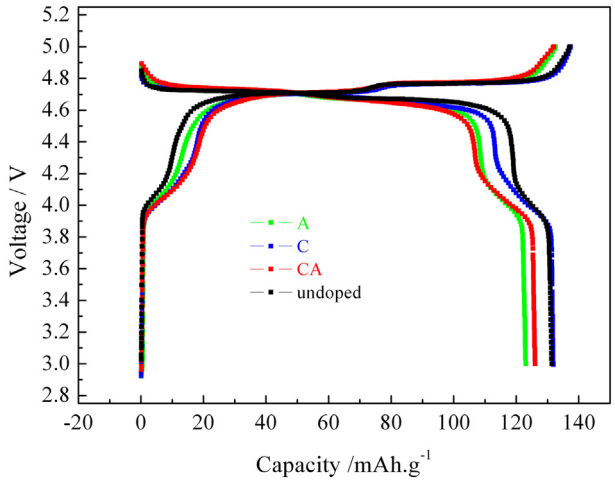

Fig. 4. Initial charge–discharge curves and differential capacity profiles of $LiNi_{0.5-x}Cu_xMn_{1.5-y}Al_yO_4$ ($x = 0, 0.05$, $y = 0, 0.05$) at 0.2 C rate. A is $LiNi_{0.5}Mn_{1.45}Al_{0.05}O_4$, C is $LiNi_{0.45}Cu_{0.05}Mn_{1.5}O_4$, and CA is $LiNi_{0.45}Cu_{0.05}Mn_{1.45}Al_{0.05}O_4$.

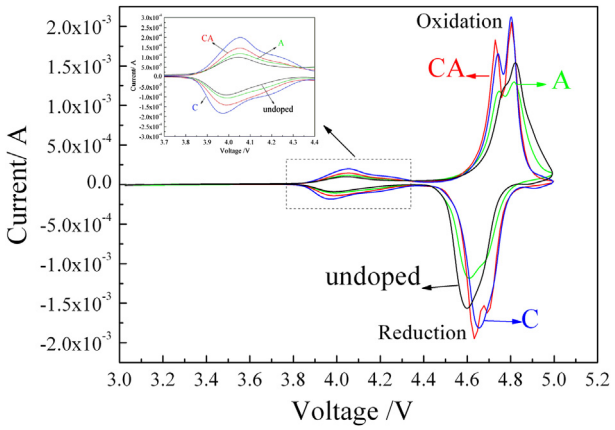

Fig. 5. Curves of cyclic voltammetry for $LiNi_{0.5-x}Cu_xMn_{1.5-y}Al_yO_4$ ($x = 0, 0.05$, $y = 0, 0.05$): A is $LiNi_{0.5}Mn_{1.45}Al_{0.05}O_4$, C is $LiNi_{0.45}Cu_{0.05}Mn_{1.5}O_4$, and CA is $LiNi_{0.45}Cu_{0.05}Mn_{1.45}Al_{0.05}O_4$.

Fig. 3 presents the particle-size distribution according to percentages of total particles vs. particle size of $LiNi_{0.5-x}Cu_xMn_{1.5-y}Al_yO_4$ ($x = 0, 0.05$, $y = 0, 0.05$) samples, which were obtained on a laser particle size analyzer. Results showed that the Cu-doped sample had the largest median particle size (namely. D50), the Al-doped sample had the smallest median particle size, and the median particle size of the Cu^{2+}/Al^{3+} co-doped sample fell between the two. These findings were consistent with the scanning electronic microscope photos. In addition, under the same calcining conditions, the undoped $LiNi_{0.5}Mn_{1.5}O_4$ powder exhibited relatively large particle size, which may suffer large resistance for Li^+ migration during charge–discharge course.

3.2. Electrochemical properties of $LiNi_{0.5-x}Cu_xMn_{1.5-y}Al_yO_4$ ($x = 0, 0.05$, $y = 0, 0.05$)

The initial charge–discharge curves of pristine $LiNi_{0.5}Mn_{1.5}O_4$ and the three doped spinel powders are shown in Fig. 4, which were obtained in a constant current charge–discharge mode between 3 and 5 V at room temperature. Undoped $LiNi_{0.5}Mn_{1.5}O_4$ had a smaller 4 V plateau (3–4.5 V) whereas other doped samples presented longer 4 V plateaus. Among these doped spinels, the Cu-doped $LiNi_{0.45}Cu_{0.05}Mn_{1.5}O_4$ sample had the largest reversible capacity of 131.9 mAh g^{-1}. The lowest discharge capacity of 123.1 mAh g^{-1} was obtained for the Al-doped $LiNi_{0.5}Mn_{1.45}Al_{0.05}O_4$ sample, which was consistent with previous research [42]. This was likely because the Al^{3+} ion is not electrochemically active, whereas the Cu^{2+} ion can be oxidated to 3+ and provides extra capacity when charging to proper potential [30]. The Cu^{2+}/Al^{3+} co-doped $LiNi_{0.45}Cu_{0.05}Mn_{1.45}Al_{0.05}O_4$ sample had moderate reversible capacity of 126.1 mAh g^{-1}, as shown in Table 2.

Between the Cu-doped $LiNi_{0.45}Cu_{0.05}Mn_{1.5}O_4$ and Cu^{2+}/Al^{3+} co-doped $LiNi_{0.45}Cu_{0.05}Mn_{1.45}Al_{0.05}O_4$, the 4 V capacity plateaus were similar, that is, 20.3 mAh g^{-1} and 21.7 mAh g^{-1}, respectively. Both were larger than the undoped sample (14.5 mAh g^{-1}) and Al-doped sample (16.4 mAh g^{-1}). The 4 V regional capacity in $LiNi_{0.5}Mn_{1.5}O_4$ was previously considered to be from Mn^{3+} oxidation induced by oxygen deficiency [43]. However, recent research has demonstrated that the Cu^{2+}/Cu^{3+} redox reaction provides extra reversible capacity between 4.2 and 4.7 V by theoretical calculation and experiments [30]. In $LiNi_{0.5-x}Cu_xMn_{1.5-y}Al_yO_4$ ($x = 0, 0.05$, $y = 0, 0.05$), the capacity provided by the Cu^{2+}/Cu^{3+} redox reaction can be calculated using the formula $C_{capacity} = (nF)/(3.6M_W)$, in which n is the number of Li^+ atoms inserted per formula unit, F = Faraday's constant (96,485 C mol^{-1}), and M_W = molecular weight of intercalated compound [39]. The calculation value of theoretical capacities from the Cu^{2+}/Cu^{3+} redox reaction of Cu^{2+} doped samples are shown in Table 2. For $LiNi_{0.45}Cu_{0.05}Mn_{1.5}O_4$ and $LiNi_{0.45}Cu_{0.05}Mn_{1.45}Al_{0.05}O_4$, the capacities from the Cu^{2+}/Cu^{3+} redox reaction were 7.33 mAh g^{-1} and 7.38 mAh g^{-1}, respectively. After this part of capacity subtracted from the total 4 V capacity, the surplus capacities attributed to the Mn^{3+}/Mn^{4+} redox reaction were not larger than those of the undoped sample. This implied that copper introduction for $LiNi_{0.5}Mn_{1.5}O_4$ may decrease the Mn^{3+} concentration. The Al^{3+} doping presented contrary results with Mn^{3+} concentration increasing for A and CA samples, as shown in Table 2.

The electrochemical behaviors of all samples prepared in this study were characterized by cyclic voltammetry with coin cells, as shown in Fig. 5. There were strong peaks at around 4.7 V, which were attributed to Ni^{2+}/Ni^{4+} redox couples. The relatively weak peaks at around 4.0 V were attributed to the redox couples of Mn^{3+}/Mn^{4+} or Cu^{2+}/Cu^{3+}. In addition, the potential differences between oxidation and reduction peaks related with the Ni^{2+}/Ni^{4+} redox reaction are listed in Table 3. The rank of $\Delta\varphi$ ($\Delta\varphi = \varphi_{oxidation} - \varphi_{reduction}$) of all samples was undoped > A > AC ~ C. The Cu-

Table 2
The ratio of 4 V capacity to the total reversible capacity for $LiNi_{0.5-x}Cu_xMn_{1.5-y}Al_yO_4$ ($x = 0, 0.05$, $y = 0, 0.05$).

Name of sample	Theoretical chemical formula	Reversible capacity/(mAh g^{-1})	5 V capacity/ (mAh g^{-1}) > 4.5 V	Total 4 V capacity/ (mAh g^{-1})	The theoretical capacity from Cu^{2+}/Cu^{3+} redox (mAh g^{-1})	The capacity of Mn^{3+}/Mn^{4+} redox[a] (mAh g^{-1})
A	$LiNi_{0.5}Mn_{1.45}Al_{0.04}O_4$	123.1	106.7	16.4	0	16.4
C	$LiNi_{0.46}Cu_{0.04}Mn_{1.5}O_4$	131.9	111.6	20.3	7.33	12.97
CA	$LiNi_{0.46}Cu_{0.04}Mn_{1.46}Al_{0.04}O_4$	126.1	104.4	21.7	7.38	14.32
Undoped	$LiNi_{0.5}Mn_{1.5}O_4$	131.4	116.9	14.5	0	14.5

[a] The capacity of Mn^{3+}/Mn^{4+} redox equals to the value that total 4 V capacity minus the capacity of Cu^{2+}/Cu^{3+} redox.

Table 3
$\Delta\varphi$ value for Ni^{2+}/Ni^{4+} redox reaction of $LiNi_{0.5-x}Cu_xMn_{1.5-y}Al_yO_4$ ($x = 0, 0.05, y = 0, 0.05$) electrodes.

Name of sample	Theoretical chemical formula	$\varphi_{oxidation}$ (mV)	$\varphi_{reduction}$ (mV)	$\Delta\varphi$ (mV)
A	$LiNi_{0.5}Mn_{1.45}Al_{0.05}O_4$	4818	4610	208
C	$LiNi_{0.45}Cu_{0.05}Mn_{1.5}O_4$	4802	4648	154
CA	$LiNi_{0.45}Cu_{0.05}Mn_{1.45}Al_{0.05}O_4$	4804	4632	172
Undoped	$LiNi_{0.5}Mn_{1.5}O_4$	4817	4591	226

doped $LiNi_{0.45}Cu_{0.05}Mn_{1.5}O_4$ and $LiNi_{0.45}Cu_{0.05}Mn_{1.45}Al_{0.05}O_4$ samples had relatively lower $\Delta\varphi$ values, which implied lower electrode polarization and higher lithium ion diffusivity in the solid state body. This phenomenon may be attributed to increases in the crystal lattice parameter and electronic conductivity for Cu^{2+}-doping in $LiNi_{0.5}Mn_{1.5}O_4$, with the larger lattice parameter allowing for easier lithium ion migration during intercalation and deintercalation course. For the Al^{3+} doped $LiNi_{0.5}Mn_{1.45}Al_{0.05}O_4$ sample, $\Delta\varphi$ was smaller than for undoped $LiNi_{0.5}Mn_{1.5}O_4$. This may be attributed to the smaller crystal size induced by Al^{3+} doping, which results in the Li^+ ion undergoing lower migration barrier during charge–discharge course.

Power pulse area-specific-impedance (ASI) can be used to evaluate power input or output performance, which reflects overall impedance change information, including electrode polarization, ohmic drop, and Li^+ ions diffusion through solid state materials during lithium ion intercalation and extraction [44]. The ASI was determined according to the expression $(A\Delta V)/I$, where A is the cross-sectional area (1.539 cm^2), ΔV is the voltage variation during current interruption for 10 s at each state of charge (SOC), and I is the current applied during testing. The ASI curve of the $Li/LiNi_{0.5-x}Cu_xMn_{1.5-y}Al_yO_4$ coin cells as a function of SOC are shown in Fig. 6. All doped samples had lower ASI values compared with undoped $LiNi_{0.5}Mn_{1.5}O_4$. This suggested that cation doping spinel can effectively decrease the direct current resistance for $LiNi_{0.5}Mn_{1.5}O_4$ during the charge–discharge course. For the Cu^{2+} doped spinel, the lowest overall impedance was attributed to largest electronic conductivity and crystal parameter, which promoted electrochemical reaction speed. For the Al^{3+} doped sample, the low ASI value was attributed to the smallest particle size, which reduced Li^+ migration length.

The cyclic curves of the spinel samples at 1 C rate at 25 °C are shown in Fig. 7. All doped samples exhibited better cyclic performance than undoped $LiNi_{0.5}Mn_{1.5}O_4$, and almost similar cycling

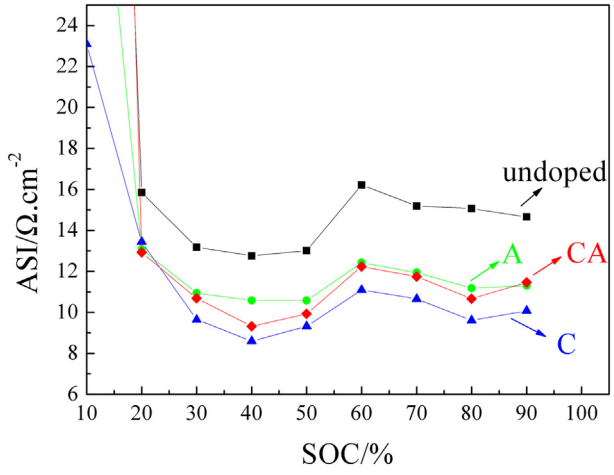

Fig. 6. Area special impedance vs. state of charge for $Li/LiNi_{0.5-x}Cu_xMn_{1.5-y}Al_yO_4$ ($x = 0, 0.05, y = 0, 0.05$) coin cell. A is $LiNi_{0.5}Mn_{1.45}Al_{0.05}O_4$, C is $LiNi_{0.45}Cu_{0.05}Mn_{1.5}O_4$, and CA is $LiNi_{0.45}Cu_{0.05}Mn_{1.45}Al_{0.05}O_4$.

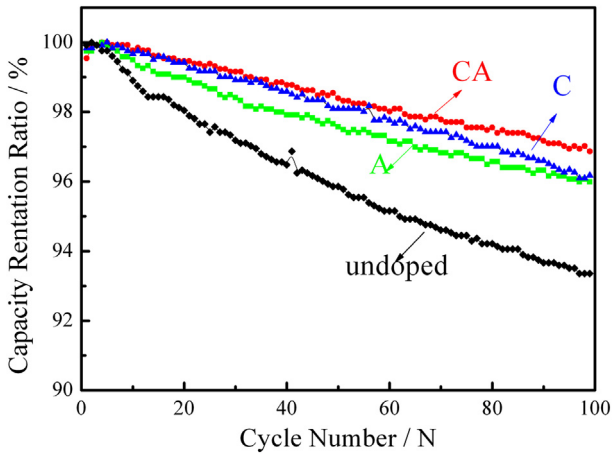

Fig. 7. Cyclic curves of the $LiNi_{0.5-x}Cu_xMn_{1.5-y}Al_yO_4$ ($x = 0, 0.05, y = 0, 0.05$) at 25 °C. The cycling tests were carried out at 1 C rate. A is $LiNi_{0.5}Mn_{1.45}Al_{0.05}O_4$, C is $LiNi_{0.45}Cu_{0.05}Mn_{1.5}O_4$, and CA is $LiNi_{0.45}Cu_{0.05}Mn_{1.45}Al_{0.05}O_4$.

stability. After 100 cycles, the discharge capacity of undoped $LiNi_{0.5}Mn_{1.5}O_4$ dropped to 93.35% of the initial state. At least 96% capacity retention was obtained for all doped samples. In addition, through owning high 4 V capacity, Cu-doped $LiNi_{0.45}Cu_{0.05}Mn_{1.5}O_4$ sample showed very good cycling retention compared with Al-doped $LiNi_{0.5}Mn_{1.45}Al_{0.05}O_4$ after 100 cycles. The Al–O bond has stronger bond energy than Mn–O and Ni–O [12], thus Al^{3+} doping can enhance the stability of the spinel skeleton structure and Cu doping in $LiNi_{0.5}Mn_{1.5}O_4$ can effectively increase electronic conductivity and Li^+ ion diffusion ability. These factors make Al^{3+} or Cu^{2+} doped samples achieve good cycle properties. However, because the Cu–O bond energy is relatively small (269 kJ mol^{-1}) [45], $LiNi_{0.45}Cu_{0.05}Mn_{1.5}O_4$ may not be the most ideal. Among the doped samples, the Cu^{2+}/Al^{3+} co-doped $LiNi_{0.45}Cu_{0.05}Mn_{1.45}Al_{0.05}O_4$ showed the best cycle performance with slight superiority and the average capacity fading rate was approximately 0.03% per cycle. It is well-known that the cyclic performance of an electrode is an integrative parameter affected by many factors, such as electronic conductivity, Li^+ ion diffusion, and bonding energy. Due to the different effects of electrochemical property improvements between Al^{3+} doping and Cu^{2+} doping, the best cyclic performance of the Cu^{2+}/Al^{3+} co-doped $LiNi_{0.45}Cu_{0.05}Mn_{1.45}Al_{0.05}O_4$ may be attributed to a combination of improvement.

4. Conclusions

We successfully prepared $LiNi_{0.5-x}Cu_xMn_{1.5-y}Al_yO_4$ ($x = 0, 0.05, y = 0, 0.05$) powders in this study. Compared to pristine $LiNi_{0.5}Mn_{1.5}O_4$, the CV, ASI and cycle results demonstrated that cyclic performance was improved by cation doping of $LiNi_{0.5}Mn_{1.5}O_4$ not only by Al^{3+} or Cu^{2+} doping but also by Al^{3+}/Cu^{2+} co-doping. The single Cu-doped $LiNi_{0.45}Cu_{0.05}Mn_{1.5}O_4$ exhibited the highest reversible capacity and electronic conductivity. The smallest crystal lattice parameter and particle size appeared in the Al-doped $LiNi_{0.5}Mn_{1.45}Al_{0.05}O_4$. The best cyclic performance was obtained in the Al^{3+}/Cu^{2+} co-doped $LiNi_{0.5}Mn_{1.45}Al_{0.05}O_4$.

Acknowledgments

This work was financially supported by the National High-Tech Research and Development (863) Plan of China (No. 2011AA1 1A230).

References

[1] N.N. Wu, D.J. Yang, J.H. Liu, W.H. Tian, Electrochim. Acta 62 (2012) 91.
[2] X.Q. .Wang, T. Osamu, K. Masaya, H. Kiroaki, J. Power Sources 168 (2007) 282.
[3] K. Teruaki, U. Kazuyoshi, T. Kenji, S. Mineo, J. Power Sources 167 (2007) 499.
[4] B.J. Hwang, R. Santhanam, S.G. Hu, J. Power Sources 108 (2002) 250.
[5] T. Yamada, T. Abe, Y. Iriyama, Z. Ogumi, Electrochem. Commun. 5 (2003) 502.
[6] T. Ohzuku, M. Kitagawa, T. Hirai, J. Electrochem. Soc. 137 (1990) 769.
[7] M.M. Thackeray, Prog. Solid State Chem. 1 (1997) 25.
[8] S. Kobayashi, I.R.M. Kottegoda, Y. Uchimoto, M. Wakihara, J. Mater. Chem. 14 (2004) 1843.
[9] F.K. Shokoohi, J.M. Tarascon, B.J. Wilkens, Appl. Phys. Lett. 59 (1991) 1260.
[10] K.H. Hwang, S.H. Lee, S.K. Joo, J. Electrochem. Soc. 141 (1994) 3296.
[11] K. .Shinichi, O. .Kenichi, S.T. Myung, N. Kumagai, T. Kamiyam, Solid State Ionics 149 (2002) 47.
[12] Y.K. Sun, O. Bookeun, H.J. Lee, Electrochim. Acta 46 (2000) 541.
[13] M.Y. Cho, K.C. Roh, S.M. Park, J.W. Lee, Mater. Lett. 65 (2011) 2011.
[14] D. Guyomard, J.M. Tarascon, J. Electrochem. Soc. 139 (1992) 937.
[15] Y.J. Kang, J.H. Kim, Y.K. Sun, J. Power Sources 146 (2005) 237.
[16] H. Kawai, M. Nagata, H. Kageyama, H. Tukamoto, A.R. West, Electrochim. Acta 45 (1999) 315.
[17] Y.E. Eli, W.F. Howard, S.H. Liu, S. Mukerjee, J. Mcbreen, J.T. Vaughey, M.M. Thackeray, J. Electrochem. Soc. 145 (1998) 1238.
[18] H. Shigemura, H. Sakaebe, H. Kageyama, H. Kobayashi, A.R. West, R. Kanno, S. Morimoto, S. Nasu, M. Tobuchi, J. Electrochem. Soc. 148 (2001) A730.
[19] C. Sigala, D. Guyomard, A. Verbaere, Y. Piffard, M. Tournoux, Solid State Ionics 81 (1995) 167.
[20] K. Amine, H. Tukamoto, H. Yasuda, Y. Fujita, J. Power Sources 68 (1997) 604.
[21] Q. Zhong, A. Bonakdarpour, M. Zhang, Y. Gao, J.R. Dahn, J. Electrochem. Soc. 144 (1997) 205.
[22] K. Kanamura, W. Hoshikawa, T. Umegaki, J. Electrochem. Soc. 149 (2002) A339.
[23] T.F. .Yi, Y.R. Zhu, R.S. Zhu, Solid State Ionics 179 (2008) 2132.
[24] Y. Idemoto, H. Narai, N. Koura, J. Power Sources 119 (2003) 125.
[25] J.H. Kim, S.T. Myung, C.S. Yoon, S.G. Kang, Y.K. Sun, Chem. Mater. 16 (2004) 906.
[26] C.M. Julien, F. Gendron, A. Amdouni, M. Massot, Mater. Sci. Eng. B 130 (2006) 41.
[27] Y.K. Sun, K.J. Hong, J. Prakash, K. Amine, Electrochem. Commun. 4 (2002) 344.
[28] S. Park, K. Park, Y. Sun, K. Nahm, Y. Lee, M. Yoshio, Electrochim. Acta 46 (2001) 1215.
[29] J. Molendaa, J. Marzeca, K.S. Wierczeka, W. Ojczyka, M. Ziemnickia, M. Molendab, M. Drozdekb, R. Dziembajb, Solid State Ionics 171 (2004) 215.
[30] M.C. Yang, B. Xu, J.H. Cheng, C.J. Pan, B.J. Hwang, Y.S. Meng, Chem. Mater. 23 (2011) 2832.
[31] F. Bonino, S. Panero, D. Satolli, B. Scrosati, J. Power Sources 97 (2001) 389.
[32] S.A. Manuel, N.G. Renganathan, S. Gopukumar, V. Subramanian, R. Bobba, Solid State Ionics 175 (2004) 291.
[33] R. Alcantara, M. Jaraba, P. Lavela, J.M. Lloris, V.C. Perez, J.L. Tirado, J. Electrochem. Soc. 152 (2005) A13.
[34] R.M. Rojas, J.M. Amarilla, L. Pascual, J.M. Rojo, D. Kovacheva, K. Petrov, J. Power Sources 160 (2006) 529.
[35] H. Şahan, H. Göktepe, Ş. Patat, Inorg. Mater. 44 (2008) 420.
[36] Y.S. Lee, Y.K. Sun, S. Ota, T. Miyashita, M. Yoshio, Electrochem. Commun. 4 (2002) 989.
[37] J.C. Arrebola, A. Caballero, M. Cruz, L. Hernán, J. Morales, E. Rodríguez Castellón, Adv. Funct. Mater. 16 (2006) 1904.
[38] J. Cabana, M.C. Cabanas, F.O. Omenya, N.A. Chernova, D.L. Zeng, M.S. Whittingham, C.P. Grey, Chem. Mater. 24 (2012) 2952.
[39] H. Göktepe, H. Şahan, Ş. Patat, A. Ülgen, Ionics 15 (2009) 233.
[40] Z.H. Tang, Z.X. Wang, X.H. Li, W.J. Peng, J. Power Sources 208 (2012) 237.
[41] T.F. Yi, Y.R. Zhu, R.S. Zhu, L. Zhou, P. Li, J. Shu, Ionics 15 (2009) 177.
[42] G.B. Zhong, Y.Y. Wang, Z.C. Zhang, C.H. Chen, Electrochim. Acta 56 (2011) 6554.
[43] S.B. Park, W.S. Eom, W.I. Cho, H. Jang, J. Power Sources 159 (2006) 679.
[44] S.H. Park, S.H. Kang, I. Belharouak, Y.K. Sun, K. Amine, J. Power Sources 177 (2008) 177.
[45] H.P. Feng, J.Y. Lin, Y.Y. Wang, C.C. Wan, J. Electrochem. Soc. 155 (2008) H620.